Physica Medica xxx (xxxx) xxx

Contents lists available at ScienceDirect

Physica Medica

journal homepage: www.elsevier.com/locate/ejmp

Original paper

A single centre intercomparison between commercial treatment planning systems for ^{90}Y radioembolization using virtual and experimental phantoms

Giuseppe Della Gala [a,1], Miriam Santoro [a,1], Garoson Albertine Rasoatsaratanany [a,b], Giulia Paolani [a], Silvia Strolin [a], Lidia Strigari [a,*]

[a] Department of Medical Physics, IRCCS Azienda Ospedaliero-Universitaria di Bologna, 40138, Bologna, Italy
[b] International Center for Theoretical Physics (ICTP), Strada Costiera, 11, 34151, Trieste, Italy

ARTICLE INFO

Keywords:
Treatment planning system
Harmonisation
TARE
Dosimetry
Virtual phantoms

ABSTRACT

Introduction: Dedicated Treatment Planning Systems (TPSs) were developed to personalize ^{90}Y-transarterial radioembolization. This study evaluated the agreement among four commercial TPSs assessing volumes of interest (VOIs) volumes and dose metrics.

Methods: A homogeneous (EH) and an anthropomorphic phantom with hot and cold inserts (EA) filled with ^{99m}Tc-pertechnetate were acquired with a SPECT/CT scanner. Their virtual versions (VH and VA, respectively) and a phantom with activity inside a single voxel (VK) were generated by an in-house MATLAB script. Images and delineated VOIs were imported into the TPSs to compute voxel-based absorbed dose distributions with various dose deposition approaches: local deposition method (LDM) and dose kernel convolution (DKC) with/without local density correction (LDC). VOI volumes and mean absorbed doses were assessed against their median value across TPSs. Dose-volume histograms (DVHs) and VK-derived dose profiles were evaluated.

Results: Small (<2.1 %) and large (up to 42.4 %) relative volume differences were observed on large (>500 ml) and small VOIs, respectively. Mean absorbed doses relative differences were < 3 % except for small VOIs with steep dose gradients (up to 89.1 % in the VA Cold Sphere VOI). Within the same TPS, LDC negligibly affected the mean absorbed dose, while DKC and LDM showed differences up to 63 %. DHVs were mostly overlapped in experimental phantoms, with some differences in the virtual versions. Dose profiles agreed within 1 %.

Conclusion: TPSs showed an overall good agreement except for small VOI volumes and mean absorbed doses of VOIs with steep dose gradients. These discrepancies should be considered in the dosimetry uncertainty assessment, thus requiring an appropriate harmonization.

1. Introduction

The transarterial radioembolization (TARE) with ^{90}Y-loaded microspheres is a well-established targeted radiotherapy procedure for the treatment of primary or secondary liver cancer based on the intra-arterial injection of radioactive compounds. Currently, two types of medical devices have been registered for this purpose, including ^{90}Y-loaded glass (TheraSphere^{TM}, Boston Scientific) and resin (Sir-Spheres, Sirtex) microspheres, that differ in terms of physical properties such as microsphere-specific activity, number of microspheres per injection, and microspheres size, and pre-injection compound preparation [1].

TARE is a non-standardized treatment, thus requiring a personalized dosimetry that follows the European Association of Nuclear Medicine (EANM) dosimetry committee guidelines [2,3].

Briefly, the therapy is preceded by a safety simulation procedure based on the injection of macro aggregated albumin (MAA) marked with ^{99m}Tc, that can be used for the assessment of the lung shunt fraction (LSF), which represents the percentage of injected activity that flows

Abbreviations: DKC, Dose kernel convolution; DVH, Dose-volume histogram; EANM, European Association of Nuclear Medicine; FWHM, Full width at half maximum; HCC, Hepatocellular Carcinoma; IEC, International Electrotechnical Commission; IQ, Image Quality; LDC, Local density correction; LDM, Local deposition method; LSF, Lung shunt fraction; MAA, Macroaggregated albumin; MC, Monte Carlo; NEMA, National Electrical Manufacturers Association; TARE, Transarterial radioembolization; TPS(s), Treatment planning system(s); VOI(s), Volume(s) of interest.

* Corresponding author.
E-mail address: lidia.strigari@aosp.bo.it (L. Strigari).

[1] These authors contributed equally to this work and share first authorship.

https://doi.org/10.1016/j.ejmp.2023.103172
Received 20 August 2023; Received in revised form 30 October 2023; Accepted 14 November 2023

towards the lungs. The acquisition of a ^{99m}Tc-based SPECT/CT image allows in addition to perform the pre-treatment dosimetry and to personalize the prescription of ^{90}Y activity based on patient and tumour specifics. The TARE procedure is then followed by a ^{90}Y PET/CT or bremsstrahlung SPECT/CT for the post-treatment verification of microspheres distribution (i.e., post-treatment dosimetry).

In the past, the lack of dedicated softwares [4] was identified as one of the main limitations for setting up a molecular radiotherapy dosimetry service, but the panorama has rapidly changed in the last years, where several treatment planning systems (TPSs) for internal dosimetry have been developed and are now commercially available [5].

TPSs are not a methodology that is strictly required by EANM dosimetry committee, as only image co-registration, volumes of interest (VOIs) drawing tools and relative activity quantification are necessarily needed, and they are usually available on SPECT and PET workstations [2] or in free available software (e.g., ImageJ [6], 3Dslicer [7]). Nevertheless, TPSs provide additional tools to the user that standardize, guide, and report the dosimetric process/workflow, such as tumour or organs contouring tools, the availability of rigid or deformable image registration systems [8], the dose deposition algorithm and the absorbed dose evaluation. More in detail, several tools are available for the aforementioned purposes. These include DICOM image and contours management, VOIs segmentation tools, absorbed dose calculation through dose deposition algorithm, results display and reporting, and, in some cases, absorbed dose distributions export in DICOM RTdose format [5]. TPSs can be used to personalize the administrable activity to patients that optimize dose distributions to treat disease and minimize dose to the healthy tissues with benefit on patient survival after TARE treatment [9]. In addition, they can be used to verify the absorbed dose distribution after treatment and the agreement with the ^{99m}Tc-MAA procedure [10]. Finally, TPSs pave the way towards the application of voxel dosimetry.

Although several homemade solutions have been proposed in the last years [11–17], TPSs that are dedicated to be used in a clinical context must be considered as medical devices and, as such, commercialized under the regulatory framework of the European Union Medical Devices Regulation 2017/745 since May 2021 [18].

Nevertheless, the implementation of these TPSs could lead to a non-negligible impact on the resulting absorbed dose distribution estimation and interpretation. Furthermore, TPS equipment must be commissioned before clinical use to avoid systematic errors and ensure treatment quality, as it is established in external beam radiotherapy [19]. Nevertheless, as the TPS use in therapy increased, a procedure for harmonization or guidelines on commissioning of these software is still lacking for TARE treatment and in general for molecular radiotherapy. The aim of this study is to compare the agreement in terms of volumes and mean absorbed doses of user-defined VOIs in ad hoc developed virtual and experimental phantoms among four TARE-dedicated TPSs.

2. Materials and methods

2.1. Treatment planning systems

Four commercial TPSs reported in Table 1 were used for the intercomparison on both experimental and virtual phantoms: Planet® Dose (DOSIsoft SA, Cachan, France; in the following, PlanetDose), MIM SurePlan™ Liver Y90™ (MIM Software Inc., Cleveland, OH; in the following, SurePlan), Simplicit^{90}Y™ (Mirada Medical, Oxford, UK; in the following, Simplicity) and Velocity™ RapidSphere v4.1 (Varian Medical Systems, Palo Alto, CA, USA; in the following, RapidSphere). All software shared a common framework, which can be summarized as follows: import of DICOM images (that is, CT and SPECT or PET images), import of VOIs in DICOM RTstruct format, selection of the VOI for scaling the total counts within it to the user-defined overall injected ^{90}Y activity (in some cases referred to as normalization VOI or perfused volume), dose deposition algorithm, and dose statistics display, including dose-volume histogram (DVH). Many additional tools are offered by all systems, such as image registration or assisted contouring tools [5], but they were not investigated as they were outside the scope of this work. A brief description of each TPS is reported in the Appendix (Supplementary Material).

Table 1
List of investigated commercially available ^{90}Y TARE dosimetry software, referring versions and dose deposition approach. Abbreviations: LDM: Local Deposition Method; DKC: dose kernel convolution. *in homogenous or inhomogeneous (CT-derived density) media; **not available in the CE-marked dosimetry workflow.

TPS & Version	Manufacturer	Abbreviation	Dose deposition approach
Planet® Dose v.3.1.2	DOSIsoft SA	Planet Dose	LDM* / DKC*
Simplicit^{90}Y™ v.2.4.0	Mirada Medical	Simplicity	LDM
SurePlan™ Liver Y90™ v.7.2.0	MIM Software Inc.	SurePlan	LDM / DKC**
Velocity™ RapidSphere v.4.1	Varian Medical Systems	RapidSphere	LDM

2.2. Dose deposition algorithm

Within the common framework, some differences can be highlighted. In particular, Planet Dose allowed to choose within two possible dose deposition algorithms for voxel dosimetry: the DKC and the LDM approach [20]. In DKC, the nuclear medicine image is convolved with a pre-computed dose kernel [21], that is obtained through a Monte Carlo (MC) simulation [22]. The dose kernel is in principle voxel size dependent (i.e., the dose kernel must be specifically computed for the voxel size of the specific nuclear medicine image), although Planet Dose is able to handle different voxel sizes as described by Dieudonnè et al. [23], by resampling the dose kernel for the desired voxel size dimension.

In the LDM, no energy transport is assumed among voxels, so all the energy irradiated by the radionuclide is deposited locally (within the same voxel). As shown by Pasciak et al. [24], the cumulative DVH obtained with LDM is closer to "true" DVH obtained with MC approach when the full width at half maximum (FWHM) of the point spread function of the real imaging system is larger than the FWHM of the dose kernel [2]. This is applicable to therapeutic beta emitters such as ^{90}Y in liver tissue and SPECT or non-digital PET scanners and largely eases the dose deposition algorithm, as this is basically reduced to a simple voxel value scaling. While Planet Dose allows to choose between DKC and LDM, RapidSphere and SurePlan employ LDM algorithm in the CE-marked dosimetry workflow. In SurePlan, DKC for ^{90}Y is also implementable in the software but outside of the CE license, so this was not investigated. Finally, Simplicity allows for performing a voxel-based dosimetry with LDM and a "standard" dosimetry based on MIRD mono-compartmental formalism. Again, this option was not investigated as it resided outside of the scope of this work.

Notably, all software required to define a normalization VOI (which is sometimes referred to as the perfused liver volume, on which the activity scaling is performed), the amount of injected activity within this VOI and the percentage of activity outside it. The latter could be used in a patient setup to consider any extrahepatic shunt including the LSF, that is defined as the amount of activity which is deposited outside the perfused liver volume. During the absorbed dose calculation, the overall injected activity was always set to the same activity for all TPSs and any extrahepatic shunt was set to zero. During the image scaling to the desired activity, in any case, all software set to zero any counts (therefore, the absorbed dose) that resides outside the normalization VOI.

Finally, SurePlan, RapidSphere and Simplicity performed the absorbed dose calculation assuming a uniform liver-like tissue density, while Planet Dose could also apply a LDC in which the local density was derived by the referenced CT image using a standard calibration curve derived from Schneider et al. [25]. Specifically, the liver-like tissue has a

mass density of 1.04 g/cm^3 for SurePlan and RapidSphere, and 1.03 g/cm^3 for Simplicity and Planet Dose (when LDC is not applied).

2.3. Phantoms

Two experimental phantoms, i.e., the International Electrotechnical Commission (IEC) National Electrical Manufacturers Association (NEMA) Image Quality (IQ) and the Anthropomorphic Torso phantom, were acquired using ^{99m}Tc and used to generate three virtual phantoms (Fig. 1) as described in the following sections.

2.3.1. Experimental phantoms

The IEC NEMA IQ phantom contains six coplanar fillable spheres of different diameters (37-, 28-, 22–, 17-, 13- and 10 mm) and size ranging from 26.5 ml to 0.5 ml, and a cylindrical lung insert filled with Styrofoam beads in a homogeneous background of approximately 9.8 L.

For the experimental acquisition, all the inserts (i.e., spheres and lung insert) were removed and the phantom container, having a volume of approximately 9940 ml, was uniformly filled with 570.4 MBq of ^{99m}Tc-pertechnetate eluted from a ^{99}Mo-^{99m}Tc generator. This phantom will be referred to as Experimental Homogeneous (EH) phantom.

The Anthropomorphic Torso phantom is characterized by a liver compartment (about 1200 ml), two lung compartments filled with Styrofoam beads (about 1800 ml in total), and a spine insert (about 240 ml) in a background of approximately 10′000 ml. Two 3D-printed fillable spheres were mounted within the liver, with diameters of 5 cm (hot sphere) and 3 cm (cold sphere).

In the experimental setup, the Anthropomorphic Torso phantom, hereafter referred to as Experimental Anthropomorphic (EA) phantom, was filled with 205.5 MBq of ^{99m}Tc-pertechnetate in the liver compartment and 53.4 MBq in the 5 cm diameter sphere (referred to as hot sphere) of ^{99m}Tc-pertechnetate to obtain a hot sphere-to-background ratio of 8:1. The 3 cm diameter sphere mounted within the liver compartment was filled with water with no activity and referred to as cold sphere. Similarly, the background (i.e., the container surrounding liver, lungs, and spine inserts) was filled with plain water.

2.3.2. Image acquisition and reconstruction protocol

The acquisitions of the experimental phantoms were performed with a Discovery 670 NM/CT SPECT/CT system (GE Healthcare, Milwaukee, USA). For both experimental phantoms, the ^{99m}Tc SPECT/CT images were obtained with the clinical protocol used in our Institute for ^{99m}Tc-MAA pre-treatment image acquisition. The CT protocol consisted of helical mode with a rotation time of 0.8 s, a slice thickness of 3.75 mm, a pitch of 1.35, the scan Field of View set to large, a tube voltage of 120 kV, and a fixed tube current of 80 mA with a standard CT image reconstruction algorithm.

The SPECT images were acquired with LEHR collimator, 128x128 matrix size per projection, an acquisition time of 10 s per projection, a step increment of 3° angle/step, an energy emission window of 140.5 ± 10 keV and an energy scatter window of 120 ± 5 keV. SPECT images were reconstructed in a Xeleris Workstation (GE Healthcare, Milwaukee, USA) using the Volumetrix MI module with Ordered Subset Expectation Maximization (OSEM) algorithm with two iterations and ten subsets, Hann prefilter with a cut-off frequency of 0.9 cycles/cm, and no post filter. Attenuation correction based on CT acquisition, scattering correction and resolution recovery were applied. The reconstructed image resulted in an isotropic voxel of 4.42 x 4.42 x 4.42 mm^3.

2.3.3. Virtual phantoms

The digital version of the SPECT acquisitions of the Anthropomorphic Torso phantom and of the homogeneously filled NEMA container phantom were developed and virtually filled with a proper number of counts in each voxel, according to the VOI to which they were assigned, to obtain noiseless images reproducing a theoretical homogenous count distribution in relevant VOIs. These phantoms were named Virtual Anthropomorphic (VA) and Homogeneous (VH) Phantom, respectively. Furthermore, we also digitally created a Virtual Kernel (VK) phantom.

The development of virtual phantoms was achieved by using an in-house developed MATLAB® (R2021b, The MathWorks Inc., Natick, MA, USA) script and the DICOM header of the experimental phantom acquisitions. The phantom images generation started from VOIs delineation accordingly to the phantoms and inserts sizes and shapes. All the

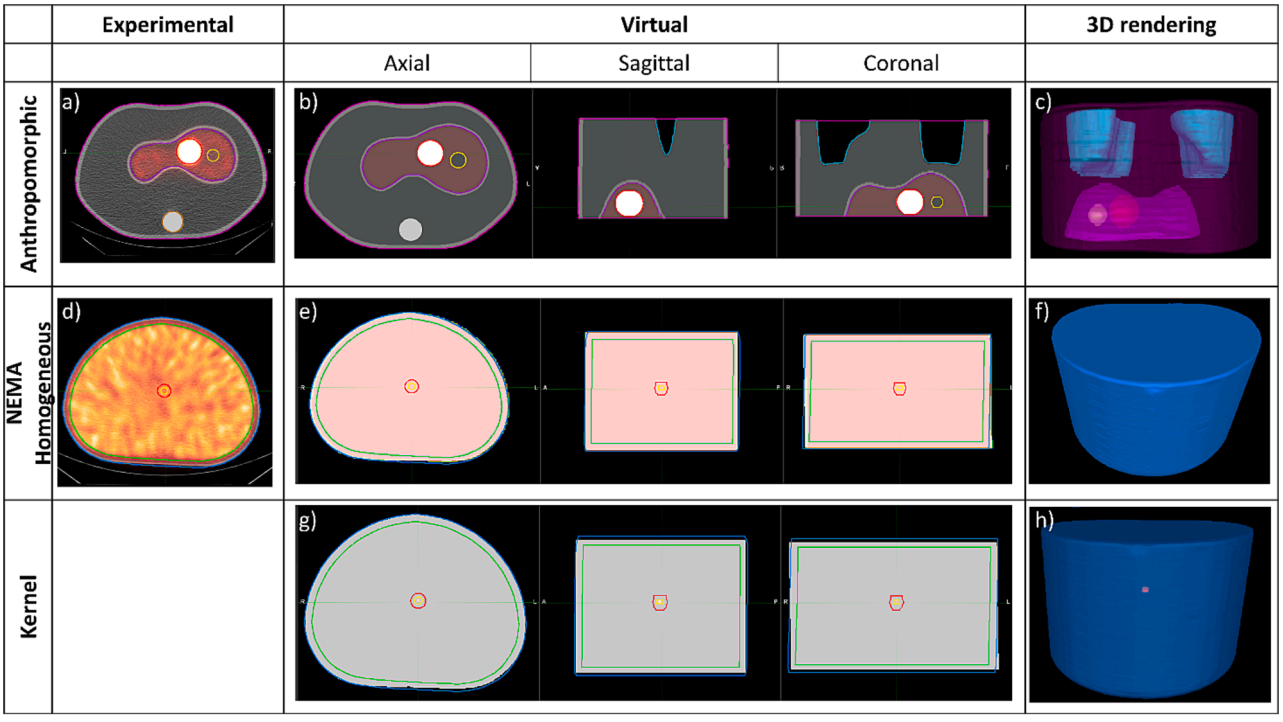

Fig. 1. Experimental (a) Anthropomorphic Torso (EA) and (d)homogenous NEMA IQ (EH) phantom acquired to generate the three Virtual (b) Anthropomorphic (VA), (e) Homogeneous (VH), and (g) Kernel (VK) phantoms. The 3D rendering of the virtual phantoms are reported in panel (c), (f), and (h).

VOIs were contoured on experimental phantoms CT images with assisted contouring tools (Whole Body and Region Grow tool) and manually refined by an experienced operator. For the generation of spherical VOIs, the 3D brush tool was used by setting the desired diameter. The VOI contouring was performed with MIM Maestro (MIM Software Inc., Cleveland, OH). The same VOIs used for the development of the virtual phantoms were considered in the dosimetric data analysis, as described in the following sections.

For each VOI, the MATLAB script generated a mask, consisting of a binary image with zeroes outside and ones inside the structure. While for the VH Phantom only one mask was needed (that is, the external shape of the NEMA IQ phantom container), the VA phantom was obtained through the superimposition of several VOIs (that is, the phantom container, the liver, and the hot and cold spheres) characterized by different activity concentrations and representing the same hot sphere-to-background ratio of 8:1 as performed with the EA Phantom. Finally, in the VK Phantom the activity was set to zero in each voxel except for one single voxel, positioned at the center of the phantom.

In each voxel with non-zero activity, the activity was set to a value of 10^6 counts (VH and Liver compartment in the VA Phantom) or $8 \bullet 10^6$ counts (hot sphere in the VA Phantom). Nevertheless, the absolute values of counts/activity in the VOIs were not relevant for absorbed dose distribution calculations as all TPSs perform an image normalization operation to the user-selected total ^{90}Y injected activity that was assumed to be equal to 1 GBq for the subsequent comparisons. For the VK phantom only, the total ^{90}Y injected activity was set to 1 MBq to be more consistent with a clinical scenario. Of note, all virtual phantoms were generated under DICOM NM modality with a voxel size of 4.42 x 4.42 x 4.42 mm^3, that is with the same voxel size as the SPECT reconstructed images.

Similarly, a virtual CT image was generated for each virtual phantom. For both VA and VH phantom, the water was replaced with the value of 0 HU, while the Lungs and Bone inserts in the VA were represented by −600 HU and 800 HU, respectively. Outside the Body VOI, −1000 HU value was applied. For the VK phantom, the same CT as the VH phantom was used. CT images where generated with a voxel size of 0.98 x 0.98 x 3.75 mm^3, as in the clinical protocol adopted in our Institution.

2.3.4. VOIs and calculated plan quality submetrics

The list and a brief description of the VOIs drawn and analysed for each phantom is reported in Table 2. The VOIs were delineated on CT images in MIM Maestro, exported from it in DICOM RTstruct format and imported in PlanetDose, RapidSphere and Simplicity softwares. After the import in the aforementioned softwares, no changes to the VOIs were applied.

VOIs volumes, mean absorbed doses and DVHs were calculated on each TPS and then exported or registered on an external datasheet. In addition, the absorbed dose at the center of each VOI was extracted and the product between mean absorbed dose, volumes and tissue density were computed to compare the product between the constant deposition among LDM algorithms and the activity within the VOI among TPSs.

Table 2
List and description of the vois analysed for each phantom.[§]This ROI was used for activity normalization purpose.

Phantom	VOI name	Description
EH/VH/VK	Body[§]	A VOI consisting of the same external NEMA IQ contour that was used for VH generation
	Body_c	A VOI consisting of the same external NEMA IQ contour that was used for the VH generation contracted by 1 cm in all directions
	Target 2	A spherical VOI of diameter of approximately 2 cm placed in the centre of the phantom
	Target 1	A spherical VOI of diameter of approximately 1 cm placed in the centre of the phantom
EA/VA	Body[§]	A VOI consisting of the same external Anthropomorphic Torso phantom contour that was used for the VA generation
	Bone	Bone insert of the Anthropomorphic Torso phantom
	Liver	Liver insert of the Anthropomorphic Torso phantom
	Lungs	Lungs insert of the Anthropomorphic Torso phantom
	Cold Sphere	Cold sphere of approximately 3 cm diameter
	Hot Sphere	Hot sphere (8:1) of approximately 5 cm diameter

2.3.5. Data analysis

For each VOI, the median value across all the TPSs in terms of VOI volumes or mean absorbed doses was reported, as well as the number of voxels included within each VOI. For each TPS, the percentage difference from the median value across systems was computed. The median value across TPSs was taken as reference as the development of a gold standard for the mean absorbed dose (such as a MC simulation) was outside the scope of this study.

The comparison between the extracted DVHs for the smallest VOIs in the EA/VA phantoms (i.e., Cold and Hot Sphere) was reported. Since the DVH of the RapidSphere TPS was not available in.csv format, the DICOM RTdose file was imported in SurePlan and DVH was computed using this TPS.

Finally, for the VK we also compared the absorbed dose profiles along one dimension on a line passing through the voxel containing the activity (i.e., corresponding to the maximum absorbed dose). Absorbed dose distributions were extracted in DICOM RTdose format and the absorbed dose profile was obtained with a homemade MATLAB® script. This analysis was not performed for Simplicity software as it did not allow to export the absorbed dose distribution in DICOM RTdose or any other usable format. The maximum dose value (i.e., the absorbed dose peak in the centre of the VK phantom) and the raw integral dose (i.e., the sum of the absorbed dose of each voxel) were obtained and reported.

3. Results

3.1. VOIs volumes

In Table 3 the median volumes across all the investigated TPS for each VOI and the relative differences from the median values for each TPS are reported.

The EH/VH/VK phantoms VOIs resulted in same volume values as the same DICOM RTstruct file was used. The same applies to EA/VA. The estimated volumes of Body and Body_c VOIs were within 2 % from the median value for all the TPSs. Generally, Simplicity and RapidSphere tended to underestimate the median volume value, while Planet Dose and SurePlan to overestimate it. Larger volume discrepancies, up to 42.4 % compared to the median volume, were observed for the smallest VOI, corresponding to Target 1. Specifically, the lowest value registered for this VOI was obtained from RapidSphere and Simplicity, both differing by −8.3 %, while the highest value was observed in Planet Dose, differing by 42.4 %.

Similar results were found for the anthropomorphic phantoms, where all the large (>500 cc) VOIs resulted in relative differences well within 2.1 % (more specifically, within 1 % for Body VOI and within 2.1 % for Liver VOI). As for the EA/VA/VK phantoms, in almost all the investigated VOIs Simplicity and RapidSphere underestimated the volume, while SurePlan and Planet Dose overestimated it. Moreover, Simplicity calculated the smaller values for the Cold and Hot spheres, reaching discrepancies up to −2.0 %, while Planet Dose computed the larger ones, reaching discrepancies up to 4.4 %.

The number of pixels included in each VOI were provided by all the TPSs except for Simplicity, for which it was calculated by dividing the VOI volume for the CT voxel size since the RTstruct are associated to the anatomical planning image (i.e., the CT). The discrepancy observed between RapidSphere and Simplicity compared to SurePlan and Planet Dose is caused by the image modality (and therefore the voxel size) to

Table 3
Median volume and number of voxel within each VOI across the investigated TPSs and relative volume differences for each TPS for the VOIs reported in Table 1. *Calculated by considering the VOI volume and the CT voxel size (i.e., 0.98 x 0.98 x 3.75 mm).

Phantom	VOI	Median Volume (cc)	Relative volume difference (%)				# Voxels			
			SurePlan	Planet Dose	Simplicity	Rapid Sphere	SurePlan	Planet Dose	Simplicity	Rapid Sphere
EH/VH/VK	Body	10095.5	−1.2 %	−0.2 %	0.5 %	0.2 %	115,687	116,793	2815799*	2,829,870
	Body_c	7641.7	0.6 %	1.6 %	−0.6 %	−0.8 %	89,137	90,007	2109232*	2,119,303
	Target 2	4.3	−4.9 %	2.3 %	2.3 %	−2.3 %	47	51	1222*	1188
	Target 1	0.5	8.3 %	42.4 %	−8.3 %	−8.3 %	7	9	139*	137
EA/VA	Body	15123.8	0.4 %	1.0 %	−0.4 %	−0.6 %	176,045	177,210	4183257*	4,205,165
	Bone	224.5	−1.5 %	4.4 %	1.0 %	−1.0 %	2565	2717	62974*	62,091
	Liver	1009.6	0.6 %	2.1 %	−0.6 %	−1.1 %	11,772	11,949	278773*	272,971
	Lungs	1877.0	0.1 %	1.8 %	−0.1 %	−0.7 %	21,791	21,464	520589*	521,319
	Cold Sphere	17.9	2.0 %	4.4 %	−2.0 %	−3.6 %	211	216	4859*	4797
	Hot Sphere	65.6	−1.0 %	2.1 %	0.6 %	−0.6 %	753	777	18326*	18,226

which the RTstruct is associated, that is CT (voxel volume: $3.6{\cdot}10^{-3}$ ml) and NM (voxel volume: $86.4{\cdot}10^{-3}$ ml), respectively.

3.2. VOIs mean absorbed doses

Table 4 shows the median value of the mean absorbed doses computed by the investigated TPSs and the relative differences from the median values for each VOI of the EH, VH, EA, and VA phantoms. For Planet Dose, the absorbed dose distribution obtained with LDM without LDC was considered as this was the same dose deposition approach used in the other TPS. A separate detailed analysis for other dose deposition algorithms available with Planet Dose are reported in later sections.

For the VH phantom, the relative mean absorbed dose difference with respect to the median value obtained across all TPS was within 3 % for almost all VOIs and TPSs. This value was exceeded only by Simplicity in the smallest VOI, that is Target 1 (-17.1 %) although this result was preceded by a warning message reporting that the VOI volume was too small and a large discrepancy (>10 %) was detected between the anatomical and the functional images.

Similarly, in the EH phantom, differences were always within 2 %, except for Simplicity for which the dose difference reached −11.5 % in Target 2 VOI. This corresponded to an absolute difference of about 0.53 Gy per GBq.

For what concerns the anthropomorphic phantoms, the discrepancy from the median value of the mean absorbed dose observed in the Body and Liver VOIs was within 2 % and 3 %, respectively. The largest discrepancies were observed for Cold Sphere in the EA phantom (from −5.2 % to + 1.3 %) and Hot Sphere in the VA phantom (from −4.4 % to + 4.0 %). An interesting behaviour was observed for the Cold Sphere VOI, where relative differences ranged between −5.2 % (Simplicity) and + 1.3 % (SurePlan) in the EA and increased up to −74.1 % (Simplicity) and + 89.1 % (SurePlan) in the VA. In absolute values, the mean absorbed doses ranged between 16.30 Gy and 17.43 Gy per GBq for the EA and between 0.70 Gy and 5.12 Gy per GBq for the VA. Nevertheless, this relatively large difference was likely due to the interpretation of the voxels positioned along the VOI edge (Fig. 2), since applying an isotropic expansion of the Cold Sphere VOI of 0.4 mm in Simplicity was sufficient to make the mean absorbed dose comparable to Planet Dose (1.23 vs 1.10 Gy, with a volume increase from 17.5 cc to 18 cc, i.e., +3%). Regarding SurePlan and RapidSphere, the large discrepancy for the Cold Sphere VOI was caused by the default method for interpolation of functional images, i.e., bicubic function, which resulted also in a smoother dose gradient.

3.3. Impact of different dose deposition algorithms within the same TPS

Table 5 summarizes the mean absorbed dose and the relative variation respect to the median absorbed doses calculated using all the dose deposition algorithms available for Planet Dose TPS.

For the EH, mean absorbed dose differences obtained with different dose deposition algorithms and with or without LDC were within 3.9 % from the median dose. As expected, mean absorbed doses obtained with LDC were slightly higher when the same dose deposition algorithm was used, since the phantom was filled with water that had a slightly lower density with respect to liver-like tissue that is assumed when LDC is not applied. In details, according to Schneider [25] the mean density of the Liver VOI obtained by the HU of the CT image was 1.022 and 1.018 g/cm^3 in the EA and VA phantoms, respectively, while the CT-derived

Table 4
Median value of the mean absorbed doses across the investigated TPSs using the LDM approach and relative mean absorbed dose differences for each TPS for the VOIs reported in Table 1. The mean absorbed dose was computed assuming 1 GBq of ^{90}Y in the Body VOI and 0 % LSF.

Phantom	VOI	Mean absorbed dose (median, Gy)	Relative mean absorbed dose difference (%)			
			SurePlan	Planet Dose	Simplicity	Rapid Sphere
EH	Body	4.79	0.1 %	0.0 %	0.0 %	−1.4 %
	Body_c	5.18	−0.3 %	0.3 %	1.7 %	−0.4 %
	Target 2	4.63	0.2 %	1.0 %	−11.5 %	−0.2 %
	Target 1	4.62	−0.1 %	0.7 %	0.1 %	−0.4 %
VH	Body	4.70	−0.2 %	0.2 %	2.1 %	−0.5 %
	Body_c	4.84	0.0 %	0.0 %	1.2 %	−0.7 %
	Target 2	4.83	0.4 %	0.3 %	−2.6 %	−0.3 %
	Target 1	4.83	0.4 %	0.3 %	−17.1 %	−0.3 %
EA	Body	3.14	−0.7 %	0.5 %	2.0 %	−0.5 %
	Liver	38.47	−0.3 %	0.3 %	2.9 %	−0.3 %
	Cold Sphere	17.20	1.3 %	0.2 %	−5.2 %	−0.2 %
	Hot Sphere	135.01	−0.4 %	0.9 %	−1.8 %	0.4 %
VA	Body	3.19	−0.4 %	−0.8 %	0.4 %	0.4 %
	Liver	46.55	−1.9 %	0.6 %	2.9 %	−0.6 %
	Cold Sphere	2.71	89.1 %	−54.5 %	−74.1 %	54.5 %
	Hot Sphere	248.76	−4.4 %	4.0 %	2.3 %	−2.3 %

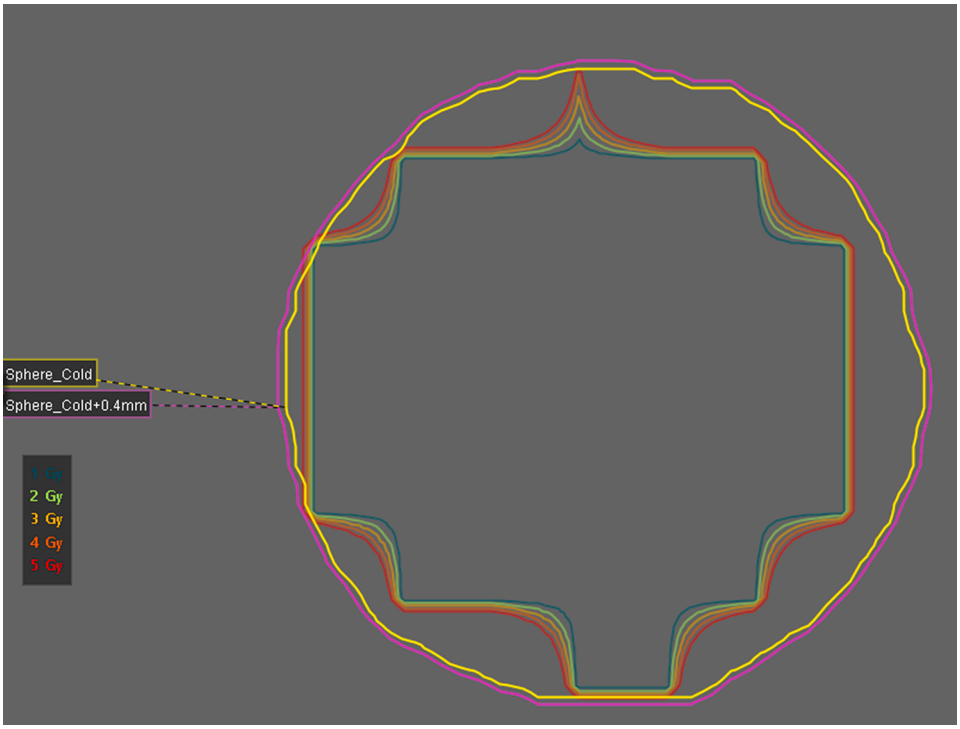

Fig. 2. Isodose lines around the Cold Sphere VOI in the VA phantom in Simplicity. A small (0.4 mm) isotropic expansion of the VOI allowed to largely recover the mean absorbed dose difference with respect to Planet Dose.

Table 5
Median value of the mean absorbed doses across the four dose deposition algorithms available in Planet Dose and relative mean absorbed dose differences for each dose deposition algorithm for the VOIs reported in Table 1. The mean absorbed dose was computed assuming 1 GBq of ^{90}Y in the Body VOI and 0 % LSF.

Phantom	VOI	Mean absorbed dose (median, Gy)	Relative mean absorbed dose difference (%) for different algorithms using Planet Dose TPS			
			LDM without LDC	DKC without LDC	LDM with LDC	DKC with LDC
EH	Body	4.70	1.8 %	−3.8 %	3.9 %	−1.8 %
	Body_c	5.10	1.9 %	−3.0 %	3.1 %	−1.9 %
	Target 2	4.60	1.9 %	−2.9 %	3.0 %	−1.9 %
	Target 1	4.57	1.8 %	−2.9 %	2.9 %	−1.8 %
VH	Body	4.75	−0.9 %	−6.7 %	8.5 %	0.9 %
	Body_c	4.75	1.9 %	−2.8 %	3.0 %	−1.9 %
	Target 2	4.76	1.8 %	−2.9 %	3.0 %	−1.8 %
	Target 1	4.76	1.8 %	−2.9 %	3.0 %	−1.8 %
EA	Body	3.08	2.4 %	−3.2 %	3.2 %	−2.4 %
	Liver	37.59	2.7 %	−3.1 %	3.1 %	−2.7 %
	Cold Sphere	17.19	0.2 %	0.1 %	−0.1 %	−0.1 %
	Hot Sphere	131.79	3.4 %	−3.6 %	3.6 %	−3.4 %
VA	Body	3.10	2.0 %	−3.6 %	2.8 %	−2.0 %
	Liver	45.25	3.5 %	−4.3 %	4.3 %	−3.5 %
	Cold Sphere	3.18	−61.2 %	60.7 %	−60.7 %	62.6 %
	Hot Sphere	245.07	5.6 %	−6.6 %	6.8 %	−5.6 %

mean density of the Body_c VOI was 1.018 g/cm^3 for both EH and VH phantoms. When compared to the liver-like tissue density of 1.03 g/cm^3, the actual density explains the reported dose differences between the same dose deposition algorithm with or without LDC in the aforementioned VOIs, which is about 1.2 %. Similarly, the LDC explained why in the EH the mean absorbed dose of the Body VOI was slightly lower than Body_c, due to the inclusion of the plastic container within the VOI. This applies also for the VH, where the virtual CT was fully represented by 0 HU values (corresponding to a density of 1.018 g/cm^3) and where the Body VOI could partially encompass voxels with zero activity and −1000 HU values. This also represents a possible explanation of the observed increase of the mean absorbed dose in the LDM with LDC with respect to LDM without LDC, which is larger for Body VOI than for the other VOIs.

For the VA, mean absorbed doses for all four dose deposition modalities varied within 4.3 % from the median dose, except for the Hot Sphere, for which discrepancies up to 6.8 % from the median dose were observed, and the Cold Sphere. In these cases, the discrepancy was between LDM and DKC approaches, as the latter generated a dose “spill-in” and “spill-out” effect (i.e., the dose due to activity outside the VOI was deposited within the VOI, and vice-versa) that did not occur with LDM. This observation is supported by the fact that small variations (within 4 %) between dose deposition algorithms were found for the same VOI in the EA, where the “spill-in/spill-out” effect is intrinsic as it is introduced by the limited resolution of the real imaging SPECT/CT system.

3.4. DVH comparison

Fig. 3 shows the DVHs of the Hot Sphere VOI in the EA (Fig. 2a) and VA (Fig. 2b) phantoms and of the Cold Sphere VOI in the EA (Fig. 2c) and VA (Fig. 2d) phantom for the investigated TPSs. For Planet Dose, the LDM without LDC was considered.

This figure highlights the impact of both TPS and real (EA) or ideal (VA) activity distributions on DVHs. Although a general good agreement among softwares was observed (as supported by the previously reported absorbed mean doses), some discrepancies were found in the high dose gradient areas that were mirrored in the DVH shapes and DVH metrics. This effect was larger on VA phantom than on EA phantom because the ideal activity distribution highlighted the difference in the interpretation of voxel that were positioned on the edges of the investigated VOIs. For example, in the VA phantom the volume of the Hot sphere VOI covered by 200 Gy (V_{200Gy}) ranged between 83.3 % (SurePlan) and 97.5 % (Simplicity). Similarly, the volume of the Cold Sphere covered by 10 Gy ranged between 2.1 % (Simplicity) and 21.2 % (RapidSphere). Notably, both RapidSphere and SurePlan DVH were computed within SurePlan since RapidSphere could not provide the DVH in.csv format. These differences in the DVH shape are furtherly commented in the discussion section. When dealing with the EA phantom, in which the activity distribution was affected by spill-in and spill-out effect, DVH became smoother and almost entirely overlapping among TPSs. In this case the exception was represented by Simplicity, that showed relevant differences in the EA Cold Sphere VOI (which was mirrored by the absorbed mean dose) and in the steepest dose gradient area (approximately between 50 Gy and 75 Gy).

3.5. Dose profiles in VK phantom

To further investigate the observed differences, in Fig. 4 we reported the absorbed dose profile extracted from the three-dimensional DICOM RTdose files on a line passing through the only voxel with non-zero activity in the VK phantom.

The maximum pixel value (i.e., the absorbed dose peak in the centre of the VK phantom) and the raw integral dose (i.e., the sum of the absorbed dose of each voxel) in a surrounding volume (±5 pixels and ±

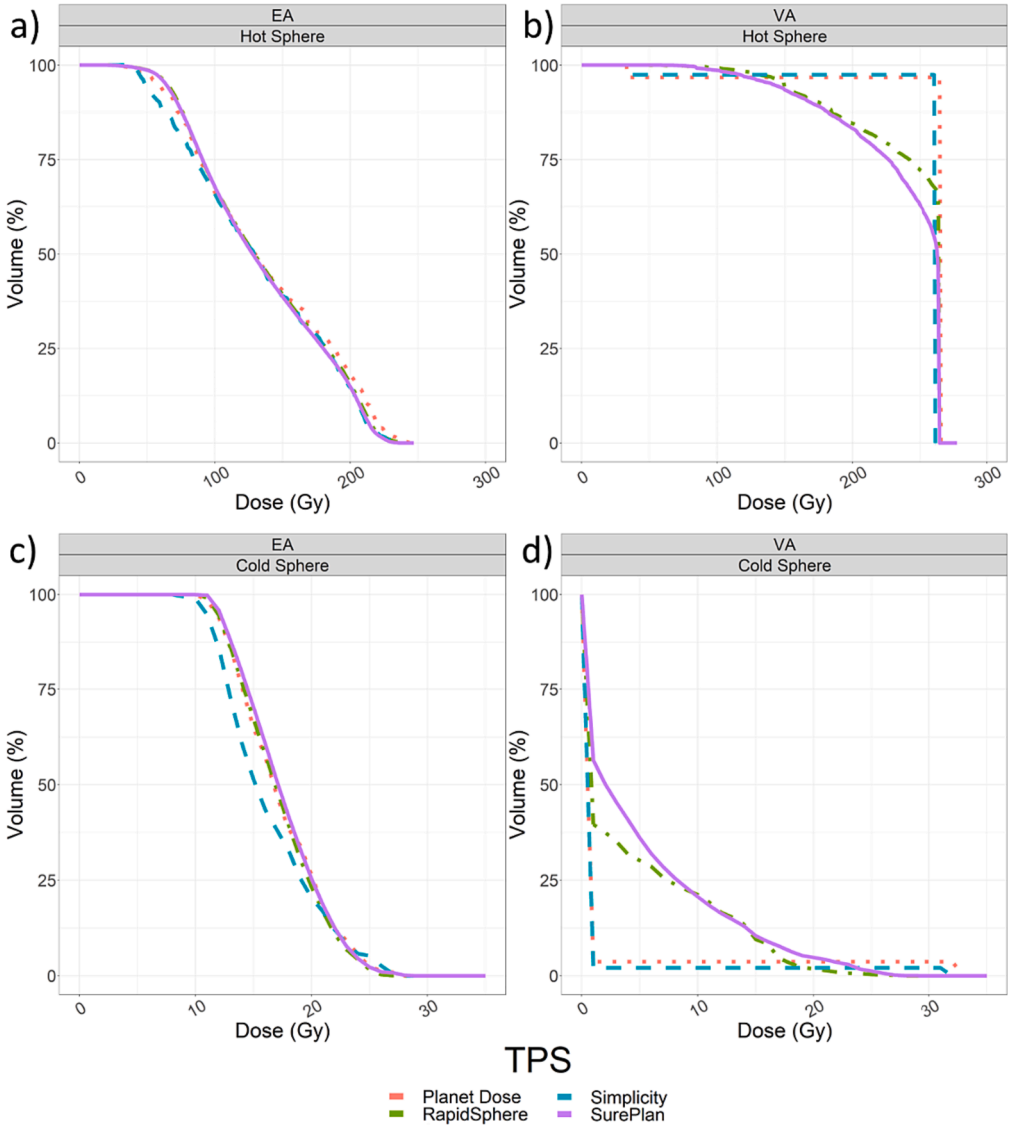

Fig. 3. DVH for hot and cold spheres for EA (panel a and c, respectively) and VA (panel b and d, respectively) phantoms. Different colours and lines indicate the investigated TPSs (e.g., Simplicity corresponds to the cyan dashed line). For Planet Dose (red dotted line), the LDM without LDC was reported. RapidSphere (green dot-dashed line) and SurePlan (violet full line) DVHs were almost entirely overlapping in Hot Sphere and Cold Sphere VOIs in VA phantom and Hot Sphere VOI for EA phantom. (For interpretation of the references to colour in this figure legend, the reader is referred to the web version of this article.)

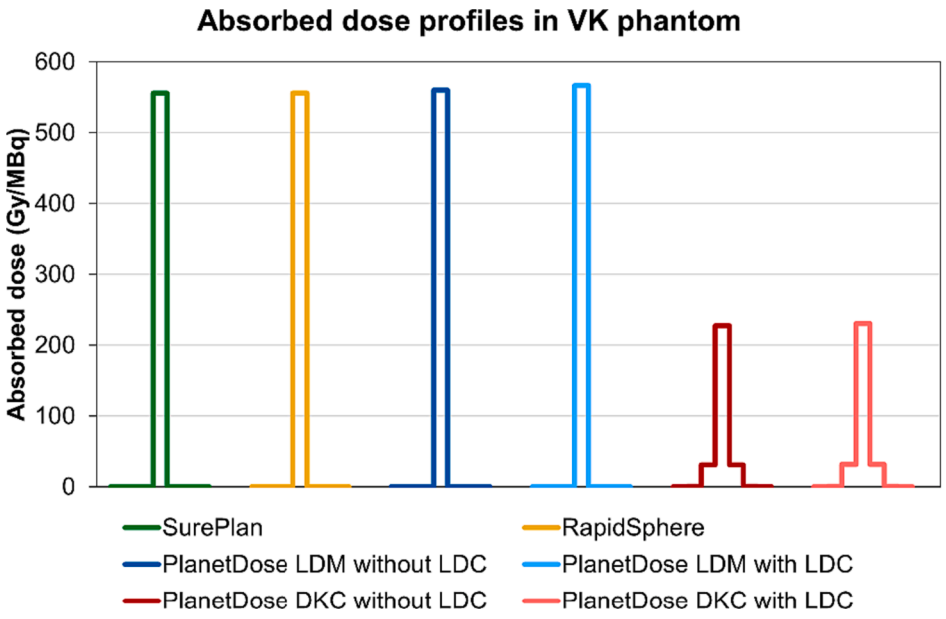

Fig. 4. Absorbed dose profiles along one dimension on a line passing through the voxel containing the activity (i.e., corresponding to the maximum absorbed dose). The available combinations of TPS and dose deposition algorithms are indicated with a different colour. The pixel size was the same (4.42 mm) for all DICOM RTdose files. Simplicity DICOM RTdose file was not available.

5 slices from the centre of the VK phantom) are reported in Table 6. The ratio between the absorbed dose in each non-zero voxel between Planet Dose DKC with LDC and Planet Dose without LDC was 1.007 ± 0.006.

Of note, the reported values for LDM were in good agreement with the mean absorbed doses estimated with the MIRD formula considering a volume of 4.42 x 4.42 x 4.42 mm^3, a constant of 49.75 Gy/MBq, and a liver-like tissue density of 1.04 g/cm^3, 1.03 g/cm^3, and 1.018 g/cm^3 that is 554.7, 560.1, and 566.0 Gy/MBq, respectively. In other terms, the constant used for the absorbed dose calculation with the local deposition resulted in 49.9 Gy/MBq (SurePlan, RapidSphere) and 49.8 Gy/MBq (Planet Dose).

3.6. Absorbed dose at the center of each VOI and product between absorbed dose, volume and tissue density

The absorbed dose at the center of each VOI was computed for SurePlan, RapidSphere, and Dosisoft (both LDM and DKC with/without LDC). Simplicity could not directly provide this metric as it does not directly support voxelized dose values. When dealing with TPSs using LDM without LDC, all data in VA and VH phantoms were in extremely good agreement (the maximum discrepancy between TPSs was always within 0.8 %) when corrected for assumed liver density. Larger differences (up to 1.3 %) were found in the EA and EH phantoms for almost all VOIs except for the Body and the Liver in the EA phantom that registered even larger discrepancies, i.e., up to 6 % and 5 %, respectively. Nevertheless, in the first case the VOI center was outside the liver compartment, that is in a region at extremely low absorbed dose, while in the latter the VOI center corresponded to a high gradient region between the Hot and Cold spheres. The same considerations apply when considering different dose deposition algorithms with/without LDC in the same TPS (i.e., LDM with/without LDC and DVK with/without LDC in Planet Dose). In addition, the DVK algorithm without LDC always led to lower absorbed doses at the center of each VOI, except for the Body VOI in the EA phantom. Detailed results are available in Table S1 (all TPSs with LDM without LDC) and Table S2 (Planet Dose LDM and DVK with/without LDC) of Supplementary materials.

The product between absorbed dose, volume, and tissue density for each VOI and TPS considering only LDM algorithms is reported in Table S3 of Supplementary materials. Similarly to the results previously presented for both volumes and mean absorbed doses, the differences were within the 2.2 % for all the VOIs having volumes > 500 cc of EH, VH, EA and VA phantoms, while increased up to 42.3 % in EH Target 1 VOI (i.e., the smallest VOI) and 96.8 % in the VA Cold Sphere VOI (i.e., where the expected absorbed dose was nearly zero and, thus, relative differences could result quite large).

4. Discussion

In this paper, the results from four commercial TPSs developed for ^{90}Y radioembolization and four algorithms within the same TPS were compared in terms of volumes and absorbed dose metrics. To our knowledge, this is the first systematic intercomparison including experimental and virtual phantoms between several commercial TPSs for ^{90}Y radioembolization dosimetry.

To calculate the absorbed dose distribution from the activity map, a full MC simulation is considered as the gold standard and can be used to validate the accuracy of the TPS absorbed dose distribution [26] or to optimize the image reconstruction protocol for absorbed dose computation purposes [27]. Even though hardwares and softwares have substantially improved, the application of MC dosimetry is still time-

Table 6
Absorbed dose in the central voxel and raw integral absorbed dose for the VK phantom in the investigated TPS (1 MBq injected activity).

	TPS and dose deposition algorithm					
	SurePlan	Rapid Sphere	Planet Dose (LDM without LDC)	Planet Dose (LDM with LDC)	Planet Dose (DKC without LDC)	Planet Dose (DKC with LDC)
Absorbed dose in the central voxel (Gy)	555.9	555.9	560.2	566.8	227.6	230.3
Raw integral absorbed dose (Gy)	555.9	555.9	560.2	566.8	534.0	540.3

consuming using patient specificities in clinical practice [21]. So additional methods such as DKC and LDM have been developed, especially for short-range β^--emitter radionuclides such as ^{90}Y and included in commercial TPSs.

However, internal dosimetry evaluation is not only limited to dose deposition algorithms and consists of a multi-step process with a specific uncertainty associated with each one of them [28] contributing to the overall absorbed dose uncertainty calculation as indicated in the EANM uncertainties guideline. One of the relevant aspects that is not fully explored regards the possible discrepancies among the TPSs available on the market and their impact on the dosimetry calculation chain.

Any dosimetric computation starts from the delineation of VOIs, so, as a first level intercomparison, the volume of user-defined VOIs were considered. The volume of an organ or tumour is generally obtained by the VOI outlined on anatomical or functional imaging data. The given outlined VOI is digitized into voxels, and its extent is defined approximately by the subset of voxels included within the boundary of the VOI [28] and by how the TPS assumes if a voxel that is crossed by the VOI boundary is included or not. In our intercomparison, large discrepancies up to about 11 % were observed for small volumes, while for larger VOIs the discrepancies were generally lower. In other words, the discrepancies in the calculation of volumes of VOIs decreased when the volume increased. These differences obtained in the statistics of VOIs suggest that TPSs incorporated different strategies in the interpretation of the same VOI (in the format of DICOM RTstruct files) for what concerns the voxels that are crossed by the VOI edges, since the number of voxels on the VOI boundary strongly decreases for increasing volumes in convex volumes. As a comparison, Kirisits et al. [29] performed a study about the accuracy of volume and DVH parameters determined with different brachytherapy TPSs. They found that the difference between volume calculation methods may lead to a 5–10 % variation in reported volumes from different TPSs, and that the methods to calculate the volumes are different between TPSs. Similar results were found in this study.

For what concerns mean absorbed doses, our study focused on the intercomparison between commercially available TPSs instead of the validation with an external system; for this reason, we did not identify a gold standard dose distribution to compare with and we rather chose the median value among the investigated TPSs as a reference. That being said, an overall good agreement between TPSs adopting the same dose deposition algorithms (i.e., LDM without LDC) was found, as the differences from the median value were within $\pm$ 3 % for the vast majority of VOIs among the investigated phantoms. The largest discrepancies were again observed for the smallest VOIs (e.g., Target 2 in EH phantom, Target 1 in the VH phantom, up to $-$11.5 % and $-$17.1 %, respectively). Another noteworthy discrepancy was found in the VA Cold Sphere, where large discrepancies up to 89.1 % from the calculated median value were observed. This highlights how the TPSs differently interpretate the voxels positioned along the VOI edge. In particular, for Simplicity an isotropic expansion of the of 0.4 mm was sufficient to reduce the mean absorbed dose difference approaching the one obtained with Planed Dose. Moreover, the MIM software introduces by default a bicubic interpolation function on functional images resulting in higher mean absorbed dose values for SurePlan and RapidSphere (whose absorbed dose distribution was imported in the MIM software).

While Simplicity, RapidSphere and SurePlan offered only one method for voxel dosimetry purpose in the CE-marked dosimetry workflow, which was basically a LDM without LDC, Planet Dose implemented also DKC and the possibility to apply a LDC based on the referenced CT image and a standard calibration curve from HU to local density. When performing an internal intercomparison between different dose deposition algorithms within Planet Dose, some trends could be identified in agreement with expectations. When comparing LDM and DKC without LDC, LDM showed systematically higher mean absorbed doses for all VOIs, except for the Body VOI in the VH phantom and the Cold Sphere VOI in the VA phantom. This effect could be traced to the dose spill-out effect of the DKC, in which the dose is not only deposited within the VOI where the radionuclide activity is identified, but also in the nearby voxels, according to the dose kernel characteristics. On the contrary, for the Cold Sphere in the VA the mean absorbed dose was significantly higher in the DKC with respect to LDM due to an absorbed dose "spill-in" effect, as the high activity voxels were outside the investigated VOI. On the same VOI the difference was smaller in the EA phantom, as the spill-in effect was already introduced in the SPECT image by the real imaging system. In addition, the impact of the LDC was evaluated within LDM or DKC approach. The LDC resulted in slightly higher mean absorbed dose in all VOIs because the CT-based density (that is, about 1.018 g/cm^3) was systematically lower than the liver-like density that is assumed when LDC is not applied (i.e., 1.03 g/cm^3).

While our study focused on virtual and experimental phantoms, Knešaurek [30] performed a study on the comparison of dose metrics based on actual patient post-treatment ^{90}Y PET/CT-based dosimetry methods, using SurePlan and Planet Dose TPSs. They highlighted that the ^{90}Y mean dose values obtained by using the investigated methods (i.e., DKC and LDM) were similar, that is approximately within 2 % on a VOI encompassing the whole liver. This agrees with our results when we consider the Liver VOI on the EA phantom, that is the VOI that is most similar to a clinical liver contour with an internal inhomogeneous activity distribution. Interestingly, when comparing LDM to DKC in the same TPS (i.e., SurePlan, in their work), they observed a slightly higher mean absorbed dose to the whole liver VOI in the DKC approach, although on average at about 3 %. On the contrary, DKC in our study showed systematically lower mean absorbed dose when compared to LDM within Planet Dose. The different behaviour might be explained by the use of clinical images with respect to phantoms, as clinical images are more likely to be affected by respiratory motion artifact or the image reconstruction algorithm characteristics. This will be object of further studies.

Differently from the aforementioned study, our study focused on virtual and experimental phantoms. Generally, the use of CT-based virtual phantoms finds application in RT both being included in automatic methods for TPS commissioning, thus reducing the potential failure modes of this process [31] and for quality control purposes [32]. Regarding the nuclear medicine field, virtual phantoms have been implemented to harmonize the standard uptake value (SUV) of different SPECT/CT scanners [33] or as theoretical benchmark/gold standard to optimize ^{90}Y PET/CT image reconstruction in terms of absorbed dose distribution accuracy [27].

In this study, the virtual phantoms allowed to better reproduce the theorical assumption of homogeneity behind the MIRD approach, avoiding noise, count inhomogeneities and possible discrepancies among machines introduced by SPECT/CT systems which still represent a non-quantitative imaging modality. Moreover, the virtual phantoms allowed to understand how the voxels, and therefore the VOI statistics, are interpreted by the TPSs in controlled and reproducible situations/experiments, including VOIs positioned across very steep gradients, which are not easy reproducible in real imaging systems. This helps to further characterize differences in voxel interpretation by TPSs, especially in high gradient areas, which are not appreciable in the experimental images of the same phantoms due to the limited resolution in the acquisition process. Finally, the virtual phantoms pave the way for the standardization of TPSs among different centres without the acquisition of phantoms images with SPECT/CT systems which can be still affected by difference in phantom preparation, image reconstruction and quantification, and correction techniques [34] although preliminary studies on SPECT/CT standardization and absolute quantification have been proposed [33–35].

We would also point out that larger discrepancies were found in small tumour-like spheres with a cold centre mimicking a tumour with a necrotic core typical of hepatocellular carcinoma (HCC) disease.

When dealing with DVH and its metrics, again an overall good agreement between TPSs was observed. In some cases, as in the reported Cold and Hot Spheres VOI in the EA and VA phantoms, some large

discrepancies in dose metrics (such as V_{10Gy} or V_{200Gy}, respectively) were observed. The discrepancies largely decreased on EA due to the image smoothing introduced by the real imaging system and DVH showed an almost complete overlap, with the previously mentioned exception of the Cold Sphere VOI in the Simplicity system. This remarks again how small VOIs dose metrics can be affected by the voxels that are positioned on the VOI edges and that 3D dosimetry derived metrics should be used with caution for this kind of volumes (i.e., small volumes with sharp absorbed dose gradients). Interestingly, the DVH generation was remarkably different in SurePlan with respect to Simplicity and Planet Dose because SurePlan by default applies bicubic interpolation on function images, thus leading to image and absorbed dose distribution smoothing. This is mirrored in the DVH shape of small VOIs characterized by steep dose gradients such as Hot Sphere in the VA phantom which results in a DVH curve that progressively bends instead of a step-based shape as in Simplicity and Planet Dose. Of note, the same behaviour was observed for SurePlan and RapidSphere absorbed dose distributions since for both TPSs DVHs were extracted from SurePlan because, as mentioned, RapidSphere could not provide the DVH in.csv format.

Finally, the absorbed dose profiles in the VK phantom were reported. The absorbed dose profiles showed the expected behaviour for LDM (in which the absorbed dose was entirely confined within one voxel) and DKC (where the dose was partially deposited in the surrounding voxels). When considering the LDM without LDC, the absorbed dose differences were negligible in terms of absorbed dose in the central voxel ($<$0.01 % between SurePlan and RapidSphere and $<$ 1 % between SurePlan or Rapid Sphere and Planet Dose), while when comparing the raw integral absorbed dose the Planet Dose DKC without LDC reached a difference of approximately + 2 % with respect to LDM without LDC within the same TPS. When applying the correction for the tissue density used in each software (i.e., when assessing the constant used for the absorbed dose calculation with the LDM) these differences were furtherly reduced to $<$ 0.2 %. This analysis highlights that the underlying LDM is substantially the same across softwares, while mean absorbed dose differences that were found in this work can be ascribed to RTstruct and dose gradients interpretation, thus especially in small volumes, in each TPS.

Our work strictly focused on the intercomparison of dosimetric results from experimental and virtual phantoms between TPS. We did not evaluate any functionality intercomparison on additional TPS tools, such as assisted contouring or image-registration tools. This will be object of further studies. For the same reason we did not provide an external validation based on a specific MC-based dose voxel kernels with the aim to compute any performance score of the investigated TPSs, as MC computation is not yet available in all clinical context. In addition, MC-based results are potentially affected by intrinsic differences such as used cross sections and selected low-energy models [36]. Thus, the reference MC code should be accurately selected.

We hope the proposed methodology can be a starting point for a shared and harmonised procedure for the commissioning of ^{90}Y radioembolization TPS within the framework of the EFOMP special interest group for radionuclide internal dosimetry (SIGFRID) and results will be reported in separate papers.

For what concerns the dose deposition algorithms, we used only the CE-marked dosimetry workflow, for some of which an external validation was already provided in literature. This is the case of SurePlan that was validated in the DKC approach against an in-house developed algorithm by Maughan et al. [37] and against the MC simulations by Balagopal and Kappadath [26]. In their work, Balagopal and Kappadath performed the validation of the SurePlan TPS against the MC simulation of 31 patients with HCC disease. They found that the mean dose calculated using the commercial software had a difference from Monte Carlo of 3 %, for both tumours and normal liver tissue. In their work, the mean absorbed dose was strongly dependent on the VOI used for the normalization, reaching a difference up to 68 % and to 73 % compared to the normalization on the entire FOV for tumour and normal tissue, respectively. This introduces the topic of the use of VOI for activity normalization that is crucial in the dosimetric process (as confirmed by Knesaurek [30]), as described in the EANM dosimetry committee guidelines [2] under the terms of perfused liver. This topic was not directly investigated in our work since the same VOI was always used for normalization purpose for all TPSs, although the interpretation of voxels positioned along the edges of the normalization VOI during the normalization step might also play a role in the explanation of the reported differences among TPSs.

5. Conclusions

In this study, the results of a dosimetric intercomparison based on experimental and virtual phantoms between several commercial TPSs for ^{90}Y radioembolization were reported. The intercomparison revealed on overall good agreement among TPSs and a fairly similar implementation of the LDM algorithm (when considering the tissue-like density correction). Non-negligible differences were identified in terms of small VOI volumes and mean absorbed dose of VOIs subject to steep dose gradients, which were furtherly emphasized through the use of in-house developed virtual phantoms. These differences should be taken into consideration in the assessment of the uncertainty in the dosimetric process. This work is proposed as an initial step towards internal dosimetry TPSs standardization and harmonization and as a possible tool for TPS commissioning in a clinical context where an external homemade validation tool is not available. Further investigations are ongoing, also involving the TPS manufacturers, to take into consideration additional tools included in the software, other radionuclides and new TPSs.

Funding

The study was partially supported by AIRC IG 20809 (2017) PI: L. Strigari.

Declaration of Competing Interest

The authors declare that they have no known competing financial interests or personal relationships that could have appeared to influence the work reported in this paper.

Acknowledgements

The authors would like to thank Matteo Mangiarotti (Varian Medical Systems), Davide Raspanti (Tema Sinergie S.p.A.), Chiara Babudri (Boston Scientifics), Cristina Silvestro (ELSE Solutions), and Angélique Rivot (DOSIsoft) for their support and comments that helped to improve the manuscript.

Appendix A. Supplementary data

Supplementary data to this article can be found online at https://doi.org/10.1016/j.ejmp.2023.103172.

References

[1] Kim SP, Cohalan C, Kopek N, Enger SA. A guide to (90)Y radioembolization and its dosimetry. Phys Med 2019;68:132–45.
[2] Chiesa C, Sjogreen-Gleisner K, Walrand S, Strigari L, Flux G, Gear J, et al. EANM dosimetry committee series on standard operational procedures: a unified methodology for 99mTc-MAA pre- and 90Y peri-therapy dosimetry in liver radioembolization with 90Y microspheres. EJNMMI Phys 2021;8:77.
[3] Sgouros G, Bolch WE, Chiti A, Dewaraja YK, Emfietzoglou D, Hobbs RF, et al. ICRU REPORT 96, dosimetry-guided radiopharmaceutical therapy. J ICRU 2021;21:1–212.
[4] Stokke C, Gabiña PM, Solný P, Cicone F, Sandström M, Gleisner KS, et al. Dosimetry-based treatment planning for molecular radiotherapy: a summary of the 2017 report from the Internal Dosimetry Task Force. EJNMMI Physics 2017;4:27.

[5] Della Gala G, Bardiès M, Tipping J, Strigari L. Overview of commercial treatment planning systems for targeted radionuclide therapy. Phys Med 2021;92:52–61.
[6] Schneider CA, Rasband WS, Eliceiri KW. NIH Image to ImageJ: 25 years of image analysis. Nat Methods 2012;9:671–5.
[7] Fedorov A, Beichel R, Kalpathy-Cramer J, Finet J, Fillion-Robin JC, Pujol S, et al. 3D slicer as an image computing platform for the quantitative imaging network. Magn Reson Imaging 2012;30:1323–41.
[8] Della Gala G, Santoro M, Paolani G, Strolin S, Cappelli A, Mosconi C, et al. How the rigid and deformable image registration approaches affect the absorbed dose estimation using images collected before and after transarterial radioembolization with 90Y resin microspheres in a clinical setting. Appl Sci 2022;12:12767.
[9] Garin E, Tselikas L, Guiu B, Chalaye J, Edeline J, de Baere T, et al. Personalised versus standard dosimetry approach of selective internal radiation therapy in patients with locally advanced hepatocellular carcinoma (DOSISPHERE-01): a randomised, multicentre, open-label phase 2 trial. Lancet Gastroenterol Hepatol 2021;6:17–29.
[10] Kafrouni M, Allimant C, Fourcade M, Vauclin S, Guiu B, Mariano-Goulart D, et al. Analysis of differences between 99mTc-MAA SPECT- and 90Y-microsphere PET-based dosimetry for hepatocellular carcinoma selective internal radiation therapy. EJNMMI Res 2019;9:62.
[11] Kletting P, Schimmel S, Hänscheid H, Luster M, Fernández M, Nosske D, et al. The NUKDOS software for treatment planning in molecular radiotherapy. Z Med Phys 2015;25:264–74.
[12] Marcatili S, Pettinato C, Daniels S, Lewis G, Edwards P, Fanti S, et al. Development and validation of RAYDOSE: a Geant4-based application for molecular radiotherapy. Phys Med Biol 2013;58:2491–508.
[13] Lehmann J, Hartmann Siantar C, Wessol DE, Wemple CA, Nigg D, Cogliati J, et al. Monte Carlo treatment planning for molecular targeted radiotherapy within the MINERVA system. Phys Med Biol 2005;50:947–58.
[14] Gardin I, Bouchet LG, Assié K, Caron J, Lisbona A, Ferrer L, et al. Voxeldoes: a computer program for 3-D dose calculation in therapeutic nuclear medicine. Cancer Biother Radiopharm 2003;18:109–15.
[15] Guy MJ, Flux GD, Papavasileiou P, Flower MA, Ott RJ. RMDP: a dedicated package for 131I SPECT quantification, registration and patient-specific dosimetry. Cancer Biother Radiopharm 2003;18:61–9.
[16] Sjögreen K, Ljungberg M, Wingårdh K, Minarik D, Strand SE. The LundADose method for planar image activity quantification and absorbed-dose assessment in radionuclide therapy. Cancer Biother Radiopharm 2005;20:92–7.
[17] Chauvin M, Borys D, Botta F, Bzowski P, Dabin J, Denis-Bacelar AM, et al. OpenDose: Open-Access Resource for Nuclear Medicine Dosimetry. J Nucl Med 2020;61:1514–9.
[18] Regulation (EU) 2017/745 of the European Parliament and of the Council of 5 April 2017 on medical devices, amending Directive 2001/83/EC, Regulation (EC) No 178/2002 and Regulation (EC) No 1223/2009 and repealing Council Directives 90/385/EEC and 93/42/EEC.
[19] Smilowitz JB, Das IJ, Feygelman V, Fraass BA, Kry SF, Marshall IR, et al. AAPM medical physics practice guideline 5.a.: Commissioning and QA of treatment planning dose calculations - megavoltage photon and electron beams. J Appl Clin Med Phys 2015;16:14–34.
[20] Forbes A, Grimon G, Esaki A, Farah J, Durand E. 90Y glass microspheres radionuclide therapy: robustness analysis with a dosimetry software. BIO Web of Conf: EDP Sci 2019:07002.
[21] Bolch WE, Bouchet LG, Robertson JS, Wessels BW, Siegel JA, Howell RW, et al. 17: The dosimetry of nonuniform activity distributions—radionuclide S values at the voxel level. J Nucl Med 1999;40:11S–36S.
[22] Lanconelli N, Pacilio M, Meo SL, Botta F, Dia AD, Aroche LAT, et al. A free database of radionuclide voxel S values for the dosimetry of nonuniform activity distributions. Phys Med Biol 2012;57:517.
[23] Dieudonné A, Hobbs RF, Bolch WE, Sgouros G, Gardin I. Fine-resolution voxel S values for constructing absorbed dose distributions at variable voxel size. J Nucl Med 2010;51:1600–7.
[24] Pasciak AS, Bourgeois AC, Bradley YC. A comparison of techniques for (90)Y PET/CT image-based dosimetry following radioembolization with resin microspheres. Front Oncol 2014;4:121.
[25] Schneider W, Bortfeld T, Schlegel W. Correlation between CT numbers and tissue parameters needed for Monte Carlo simulations of clinical dose distributions. Phys Med Biol 2000;45:459–78.
[26] Balagopal A, Kappadath SC. Characterization of (90) Y-SPECT/CT self-calibration approaches on the quantification of voxel-level absorbed doses following (90) Y-microsphere selective internal radiation therapy. Med Phys 2018;45:875–83.
[27] Hou X, Ma H, Esquinas PL, Uribe C, Tolhurst S, Bénard F, et al. Impact of image reconstruction method on dose distributions derived from (90)Y PET images: phantom and liver radioembolization patient studies. Phys Med Biol 2020;65:215022.
[28] Gear JI, Cox MG, Gustafsson J, Gleisner KS, Murray I, Glatting G, et al. EANM practical guidance on uncertainty analysis for molecular radiotherapy absorbed dose calculations. Eur J Nucl Med Mol Imaging 2018;45:2456–74.
[29] Kirisits C, Siebert FA, Baltas D, De Brabandere M, Hellebust TP, Berger D, et al. Accuracy of volume and DVH parameters determined with different brachytherapy treatment planning systems. Radiother Oncol 2007;84:290–7.
[30] Knešaurek K. Comparison of posttherapy (90)Y positron emission tomography/computed tomography dosimetry methods in liver therapy with (90)Y microspheres. World J Nucl Med 2020;19:359–65.
[31] Wexler A, Gu B, Goddu S, Mutic M, Yaddanapudi S, Olsen L, et al. FMEA of manual and automated methods for commissioning a radiotherapy treatment planning system. Med Phys 2017;44:4415–25.
[32] Denis E, Guédon J, Beaumont S, Normand N. Discrete and continuous description of a three-dimensional scene for quality control of radiotherapy treatment planning systems. SPIE 2006.
[33] Nakahara T, Daisaki H, Yamamoto Y, Iimori T, Miyagawa K, Okamoto T, et al. Use of a digital phantom developed by QIBA for harmonizing SUVs obtained from the state-of-the-art SPECT/CT systems: a multicenter study. EJNMMI Res 2017;7:53.
[34] Piwowarska-Bilska H, Supińska A, Birkenfeld B. What validation tests can be done by the clinical medical physicist while waiting for the standardization of quantitative SPECT/CT imaging? EJNMMI Phys 2022;9:8.
[35] Peters SMB, van der Werf NR, Segbers M, van Velden FHP, Wierts R, Blokland KAK, et al. Towards standardization of absolute SPECT/CT quantification: a multi-center and multi-vendor phantom study. EJNMMI Phys 2019;6:29.
[36] Pacilio M, Lanconelli N, Lo MS, Betti M, Montani L, Torres AL, et al. Differences among Monte Carlo codes in the calculations of voxel S values for radionuclide targeted therapy and analysis of their impact on absorbed dose evaluations. Med Phys 2009;36:1543–52.
[37] Maughan NM, Garcia-Ramirez J, Arpidone M, Swallen A, Laforest R, Goddu SM, et al. Validation of post-treatment PET-based dosimetry software for hepatic radioembolization of Yttrium-90 microspheres. Med Phys 2019;46:2394–402.